Title

A STUDY OF PRECIPITATION IN INTERSTITIAL ALLOYS: IV. THE PRECIPITATION SEQUENCE IN Pt-C

Authors

Westmacott, K.H.
Witcomb, M.J.
Dahmen, U.

Publication Date

1982-07-01

LBL-14777
Preprint

Lawrence Berkeley Laboratory
UNIVERSITY OF CALIFORNIA

Materials & Molecular Research Division

Submitted to Acta Metallurgica

A STUDY OF PRECIPITATION IN INTERSTITIAL ALLOYS:
IV. THE PRECIPITATION SEQUENCE IN Pt-C

K.H. Westmacott, M.J. Witcomb, and U. Dahmen

July 1982

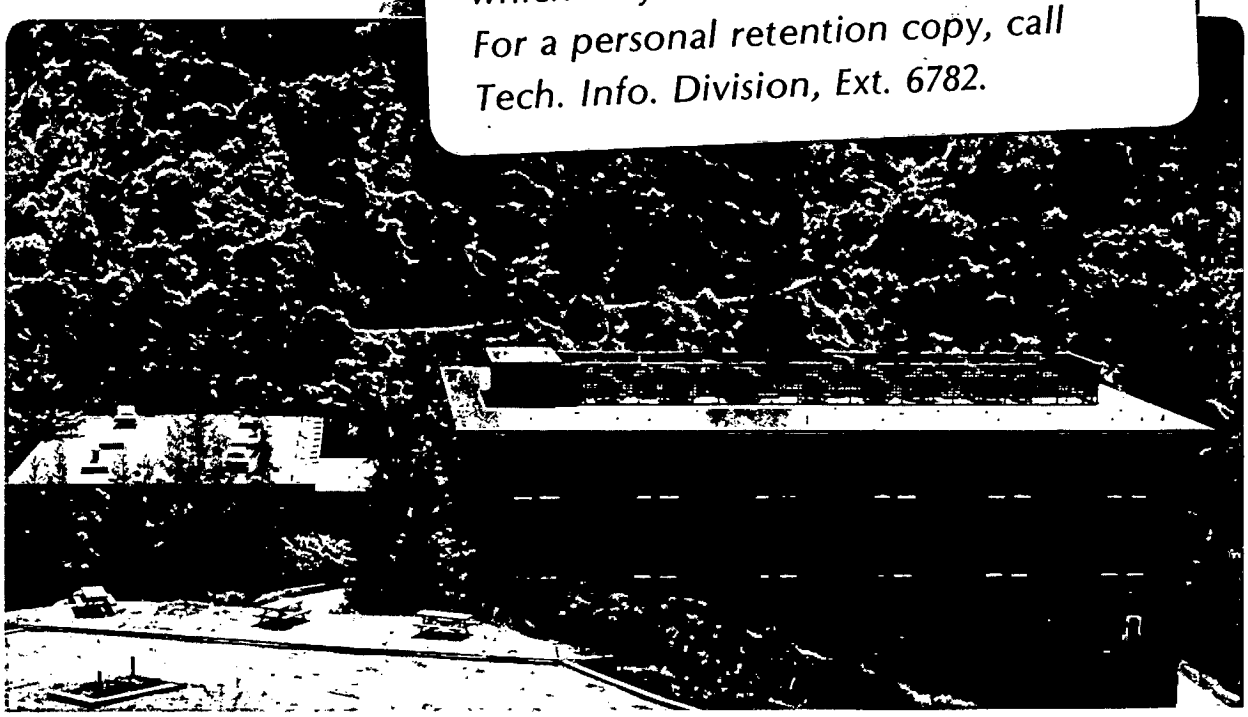

Prepared for the U.S. Department of Energy under Contract DE-AC03-76SF00098

DISCLAIMER

LBL-14777

A STUDY OF PRECIPITATION IN INTERSTITIAL ALLOYS:

IV. THE PRECIPITATION SEQUENCE IN Pt-C.

K. H. Westmacott, M. J. Witcomb*, and U. Dahmen

Materials and Molecular Research Division

Lawrence Berkeley Laboratory

University of California

Berkeley, CA 94720

---

*Electron Microscopy Unit, University of the Witwatersrand, Johannesburg, S. A.

ABSTRACT

A systematic transmission electron microscopy study of the entire carbide precipitate nucleation and growth process in quenched, aged platinum has been made. Five distinct stages have been identified in the growth sequence, four coincide with changes in the Burgers and displacement vectors and the fifth in the configuration of the precipitates. Diffraction contrast analysis has shown that all the precipitate platelets lie in {001} matrix planes, are vacancy in character and are semi-coherent. Precipitates form initially by co-precipitation of vacancies and carbon atoms and the growth sequence follows a ripening type process. At intermediate aging temperatures voids become the preferred growth sites presumably acting as vacancy sources. Various aspects of the precipitation reaction have been explained from the standpoint of the role of vacancies (V), and the system can be treated either as a Pt-C binary or a Pt-C-V ternary alloy.

INTRODUCTION

In the preceding papers (II, III) it was shown in II that Pt containing small amounts of carbon undergoes a precipitation reaction during quench-aging. One product of this reaction is a new metastable carbide phase of nominal composition Pt_2C. In paper III the concepts of coherency were extended to distinguish between two possible mechanisms of precipitate nucleation and growth, and experimental confirmation for both mechanisms was presented.

This paper describes the entire precipitation sequence in Pt-C emphasizing the atomic processes involved. The formation of the first carbide unit cell, the subsequent thickening, the transition stages, and the role of lattice defects are discussed.

The experimental procedures employed in the investigation are the same as those given in the preceding papers.

RESULTS

The Precipitate Growth Sequence

The course of the precipitation reaction has been followed through detailed contrast analyses of the dislocations bounding the precipitate. Both the displacement vector of the plate and the nature of the strain field were also determined at each step in the precipitation sequence. Additional analyses were made of the precipitates during the transition from one stage to the next in order to ensure that a consecutive succession of events was occurring.

A remarkable similarity was found between the sequence observed in the Pt-C interstitial system and that observed in the "classical" Al-Cu substitutional system. The initial decomposition of the supersaturated solid solution occurred by the formation of monolayer platelets of carbon (designated α) on the {001} matrix planes.

These precipitates were analogous to GP zones except for their semicoherent nature. As shown earlier (1), they were characterized by a bounding dislocation with Burgers vector $\underset{\sim}{b}$ and displacement vector $\underset{\sim}{R}$ of a/3 <001>. These features were attributed to the precipitates forming by a co-precipitation mechanism in which tightly bound carbon atom-vacancy complexes condensed in an {001} planar disc which then collapsed. The α zones were already formed in the as-quenched foil, probably as a consequence of the unavoidable long "tail" on the quenching rate curve of the UHV quenching technique employed.

During post-quench aging at 400°C, the second stage of precipitation (α') evolved. The precipitate habit remained {001} but $\underset{\sim}{b}$ and $\underset{\sim}{R}$ were now very close to a/2 <001>. The concentration of α' precipitates was considerably less than the α but the size (which was rather uniform) had increased. Furthermore, the shape of the plates became more angular with the straight segments lying along <110> directions. The experiments described in paper II identify the α' as a body-centered tetragonal Pt_2C carbide phase.

Continued aging in the temperature range 400-530°C resulted in a gradual coarsening of the precipitate structure, a return to a more rounded precipitate shape, and the appearance of a few different precipitates, designated α'', characterized by $\underset{\sim}{b}$ and $\underset{\sim}{R}$ of a <001>. An examination of thicker sections of Pt using the HVEM revealed that α'' developed preferentially in some regions of the foil. This is attributed to the non-uniform distribution of carbon in the sample. It was also found that further thickening of the precipitates beyond α'' occurred, but their characterization by contrast analysis became less reliable.

The final stage in the sequence occurred during long annealing at temperatures in excess of 500°C. The microstructure showed a dramatic change in that all the precipitates were now arranged in widely spaced but densely packed linear arrays.

In order to facilitate a comparison between the various precipitate stages and to obtain an understanding of their sequential development, the same contrast analysis was made for α, α', and α''. First, however, extensive preliminary experiments were performed to examine the nature of the contrast associated with the precipitates. The predictions of the dynamical theory of diffraction contrast for {111} stacking faults and dislocations were found to be valid for the {001} defects. Thus, by the selection of appropriate diffraction vectors, the precipitate character could be identified unambiguously. For example, the α precipitate contrast obeys the rules $\underset{\sim}{g}.\underset{\sim}{b} = \pm n/3$ for the dislocations; $\beta = 2\pi n/3$ for the phase angle, where n = 0,1,2, ... The dislocation associated with the (001) precipitate variant shows $\pm\frac{1}{3}$, $\pm\frac{2}{3}$, ± 1 characteristics for 111, 002, and 113 reflections respectively, while displacement fringes are observed for all three variants in the 111 reflection and for only two variants in the 113 reflection. With $\underset{\sim}{g}$ = 220, only two variants are imaged, since the third variant is out of contrast. A series of micrographs which illustrate these characteristics of the α precipitates is shown in Fig. 1.

In analyzing the α' defects, a case not yet treated theoretically is encountered. Since $\underset{\sim}{b} = \underset{\sim}{R} = \frac{a}{2}\langle 001\rangle$, the conditions $\underset{\sim}{g} \cdot \underset{\sim}{b} = \pm\frac{(n+1)}{2}$ and $\beta = (n+1)\pi$ are found. π boundaries generally occur for antiphase domain boundaries in ordered materials and are therefore not usually terminated by $\frac{a}{2}\langle 001\rangle$ dislocations. We have found that when $\underset{\sim}{g}.\underset{\sim}{b} = \pm\frac{1}{2}$ and $w \gg 0$, the dislocation exhibits contrast behavior similar to the case $\underset{\sim}{g} \cdot \underset{\sim}{b} = \pm\frac{2}{3}$ and $w \gg 0$ as illustrated in Fig. 2. It is apparent that when $\underset{\sim}{g}.\underset{\sim}{b} = +\frac{1}{2}$ (Fig. 2a), the precipitate shows "inside" contrast and the dislocation is visible, whereas with $\underset{\sim}{g}.\underset{\sim}{b} = -\frac{1}{2}$, "outside" contrast and a barely visible dislocation is observed. However, as is the case of Frank loops, the difference between $+\frac{1}{2}$ and $-\frac{1}{2}$ is somewhat masked by the displacement (or stacking fault) fringe contrast.

In the analysis of α' precipitates shown in Fig. 3, the π faults are visible with $\underset{\sim}{g}$ = 111 and 311 and invisible in 220 type reflections. The dislocations correspondingly exhibit $\pm\frac{1}{2}$ and $\pm$ 1 behavior.

The α" precipitates having $\underset{\sim}{b} = \underset{\sim}{R}$ = a<001> displacements exhibit dislocation contrast under all conditions except $\underset{\sim}{g}.\underset{\sim}{b} = 0$, and as expected, the precipitates show no fringe contrast (see precipitate marked A in Fig. 4).

From a comparison of Figs. 2-4, the contrast differences between the α, α', and α" precipitates are apparent and the assigned $\underset{\sim}{b}$ and $\underset{\sim}{R}$ vectors readily confirmed.

In addition to this analysis, the character of the precipitate strain field at each stage was determined using a simplified inside/outside contrast analysis (2). An independent check of the results of these determinations was in some instances made by examining the character of the dark field image asymmetry when $\underset{\sim}{g}.\underset{\sim}{b} = 0$ (3). In every case the precipitates produced a vacancy type strain field in the surrounding matrix.

The final microstructures to form in the precipitation sequence are seen in Fig. 5. The low magnification micrograph (Fig. 5a) illustrates the precipitate free zones around dislocations, while Fig. 5b shows the striking heterogeneous groupings which survive after the matrix precipitates dissolve. This latter structure could result from either the preferential growth of the precipitates nucleated on matrix dislocations, or the autocatalytic renucleation of the dissolving precipitates. A detailed study of this stage has not yet been made.

The Transition Processes.

Once the aging treatments for producing the α' and α" precipitates were established, further specimens were given intermediate agings to capture the transition processes. Contrast analyses on these specimens provided confirmation of the earlier results and gave further insight into the precipitate growth mechanisms.

The $\alpha \longrightarrow \alpha'$ transition analyzed in the micrographs of Fig. 6 was in its early stages after a 1 h anneal at 400°C. From a comparison of the contrast behavior of the large precipitates with those in Figs. 1 and 3, it is clear that the central regions of the α platelets are thickening to α' by the growth of a second layer. This transition is marked by a change in the displacement vector from a/3 to a/2. Since it was shown in paper II that the α' precipitates have the Pt_2C carbide structure, the change from a/3 to a/2 rather than 2/3a displacement is significant. It is explained by the structural relaxation and carbon reordering which accompany the formation of the first unit cell of carbide.

The discussion of mechanisms for further growth given in paper III showed that a number of possibilities are available for the $\alpha' \longrightarrow \alpha''$ transition and this was indeed confirmed experimentally. An example of the most commonly observed transition process is given in Fig. 7. An analysis of a precipitate intersecting the foil surfaces shows that the outer and inner regions of the precipitate plate and the bounding dislocations exhibit contrast consistent with a/2 <001> (α') and a <001> (α'') respectively. A sketch depicting this growth process is given in Fig. 7c.

One further noteworthy feature of the micrographs is the frequent observation of small voids associated with the precipitates. Although evidence indicates the voids are formed during the initial quench, their presence is best detected after a subsequent aging at 400°C when the large α' precipitates are all seen to have voids in their centers (see e.g. Fig. 6).

Preliminary Studies of Precipitate Dissolution

As a further aid to understanding the structure, behavior and stability of the precipitates, in-situ annealing studies are being conducted in a high voltage electron microscope. The advantage of this procedure is that a specific stage in the

precipitation sequence (e.g. α') can first be established by bulk annealing. Then, following thinning, the thin foil shrinkage behavior of this stage may be observed by in-situ annealing and compared directly with similar results on the other stages.

This comparison was particularly valuable for the α and α' since it provided further evidence that this is the critical transition in the sequence. Fig. 8a shows α precipitates in an as-quenched foil while Fig. 8e is a convergent beam diffraction pattern taken from an edge-on (001)α precipitate with the electron beam parallel to the [100] zone axis. The continuous streaking between the matrix spots of the diffraction pattern is the shape factor effect characteristic of thin plate precipitates such as GP zones. Figs. 8b-d are further micrographs of the same area as 8a taken from a series of exposures recorded during isothermal annealing* at 452°C (725K). It is apparent that the shrinkage of the precipitates was regular and continuous. In fact the plot of radius against time (see Fig. 8f) showed a linear relationship. The shrinkage rate obtained by averaging the rates for a number of precipitates was 0.02 nm s^{-1}.

A similar annealing experiment was performed on a foil which had been bulk aged at 515°C to form α' precipitates. The initial microstructure and convergent beam diffraction pattern from an individual precipitate are shown in Figs. 9a and e. During subsequent in-situ annealing, the shrinkage behavior illustrated in 9b-d was observed. Again, shrinkage was a linear function of time (Fig. 9f) but the temperature range necessary for achieving shrinkage rates comparable to those found for the α precipitates was significantly higher. For example, it required a

---

*To ensure that the results were not significantly perturbed by displacement damage effects (5), annealing sequences were performed at two different accelerating voltages, 650kV and 900kV, and comparative ex-situ studies were also made.

temperature of 515°C (788K) to obtain an average shrinkage rate of 0.005 nm s^{-1}. This large difference in rates or temperature is further evidence that a significant structural change had occurred during the α to α' transition.

Unequivocal proof that the α' precipitate marks the first appearance of the carbide phase is provided by a comparison of Figs. 8e and 9e. The additional spots visible as short streaks in the diffraction pattern of 9e must arise as the result of carbon ordering as the carbide structure formed.

DISCUSSION

An unusual aspect of the present study is the fact that the interstitial solute atoms participating in the precipitation reaction are present only in concentrations comparable to the quenched-in vacancy concentration. As a consequence, neither the carbon atoms nor the vacancies dominate and the microstructural development during the return to equilibrium after a rapid quench can be viewed in a number of equivalent ways. It is fruitful to discuss several of these alternate schemes since they illustrate different facets of the problem.

One approach is to focus attention on the vacancies, as in a conventional quenching experiment, and study the effect of carbon impurities on the formation of secondary defects (6). As shown in paper II, some grades of Pt (e.g. that supplied by Engelhard) exhibit "normal" behavior in that perfect prismatic loops are observed. The effects on the microstructure of increasing carbon impurity content could then be explained by the formation of Cottrell atmospheres at the dislocation loops (7) or by stabilization of {001} stacking faults by the Suzuki mechanism (8).

A second possibility is to treat carbon as a solute rather than impurity atom and when its concentration exceeds a few hundred atomic ppm, regard the system as a Pt-C binary. The logic for this is the observation that the α defects ripen and increase in complexity during post-quench aging treatments rather than simply

dissolve as would secondary defects. According to this view, the precipitation of a monolayer plate of carbon on {001} leads to an expansion of the lattice which is countered by the precipitation of an equal monolayer disc of vacancies. The net result is a semi-coherent GP zone. This disc shaped cluster of carbon could also be considered a pre-precipitate since it is a precursor to a true precipitate but has no identifiable crystal structure itself.

As shown in paper III, the nucleation and continued growth of the (α) GP zones can occur by coherent or semicoherent mechanisms. This suggests that a third, and most logical, approach is to treat the system as the Pt-C-V ternary. This is particularly appropriate in view of the demonstrated close interconnection between the fates of the solute atom and vacancy supersaturations.

If, as suggested earlier (1), the carbon atoms and vacancies form strongly bound complexes, migration of the complex as a single entity constitutes solute segregation, and clustering will result in the formation of a platinum-carbon-vacancy (Pt-C-V) "compound". Thus the three alternative views of the precipitation reaction are Pt with quenched-in vacancies, the Pt-C binary, or the Pt-C-V ternary, and each one emphasizes a different aspect. We now discuss in detail the observations on Pt-C combining these different approaches.

The perfect dislocation loops observed in the Engelhard grade of Pt are best discussed in terms of quenched in vacancies. If the stacking fault energy in pure Pt is high Frank loops on {111} planes will be metastable and the usual secondary defect will be the unfaulted perfect loop. This behavior of the pure metal is perturbed when small amounts of impurities are introduced. The effect of carbon is to change the perfect loop structure to "faulted loops", or α carbon platelets, on {001} planes. Further, if the stringent quenching environment is relaxed and small amounts of oxygen are introduced, the α precipitates are replaced by a very high density of voids

(6). This drastic change indicates that the form of the interstitial carbon is altered probably by formation of carbon-oxygen complexes which act as potent nucleation sites for voids. After ultrahigh vacuum quenching from the melting point, voids and α carbon precipitates develop simultaneously. This could be explained if the platinum contains residual oxygen of the order of 100 atomic ppm (as indicated by supplier analysis) in addition to several hundred atomic ppm carbon. During the quench from the melting point partitioning of the vacancies between the carbon and carbon-oxygen complexes would result in both carbon precipitate and void formation. This proposal is supported by the observation that voids are not visible in specimens quenched from 1250°C and the precipitate density is much lower. The smaller void size expected under this lower vacancy supersaturation, assuming the partitioning and scale of precipitation are unchanged, would make them invisible under conventional imaging conditions.

If, during a quench from the melting point the voids nucleate first, the large vacancy-carbon atom binding energy will concentrate the carbon in the regions surrounding the voids. This assumes the voids are good sinks for vacancies but not for carbon. If carbon plate nucleation then occurs uniformly throughout the matrix once the critical temperature for precipitation is reached, those precipitates near the pre-existing voids will be favored for subsequent growth. This is because during subsequent high temperature aging the matrix vacancy concentration is soon reduced to its equilibrium value and growth of precipitates remote from the voids ceases, whereas near the voids both excess carbon and a source of vacancies are available to promote further growth.

While the formation of the initial microstructure is most naturally discussed in terms of a quenching study, the subsequent formation of the metastable carbide emphasizes the aspect of a Pt-C binary alloy. The α precipitates are precursors to the formation of the carbide (α' precipitate) Pt_2C which has the same {001} habit

plane. In addition, the α platelets are similar to GP zones in that they have neither the precipitate nor the matrix structure. The vacancy collapse produces an AA stacking fault in a matrix of AB stacking. This gives the correct stacking sequence for Pt atoms in the carbide, but the carbide unit cell is incomplete since its formation requires two adjacent stacking faults and ordering of the carbon atoms. In terms of bonding, the α platelets closely approximate the coordination found in the carbide. As pointed out in paper II, the carbide structure may be regarded as a distorted fluorite structure. The coordination is 8:4 with each carbon surrounded by 8 platinum atoms in a distorted cube and each platinum at the center of a distorted tetrahedron of carbon atoms. The co-precipitation of carbon and vacancies instantly provides the correct coordination for the carbon atom by platinum with the coordinating polyhedra sharing faces in the α precipitates. The correct coordination of the carbon around the Pt atoms is established only during the transition to α', the first unit cell of the carbide. The ordered arrangement of the carbon atoms leads to the more stable edge-sharing of the coordinating polyhedra (9). This approach to the carbide precipitation from the point of view of bonding in a binary alloy system has been used successfully by Jack and Jack (10) to rationalize carbide and nitride structures in transition metals. The same reasoning applied to the Pt-C system also explains the {001} habit since the Pt coordination polyhedra of the carbide perfectly matches the {001} planes of the matrix.

In order to discuss the development of the entire precipitation sequence, especially the latter stages, it is advantageous to picture the system as a Pt-C-V ternary. The strong binding between carbon and vacancies and their presence in comparable amounts leads to their co-precipitation. With one exception, it was found that the entire sequence of nucleation and growth occurred by this co-precipitation mechanism. An α platelet formed by this mechanism is a semicoherent nucleus and a corresponding growth step is a semicoherent ledge. As shown in paper III, coherent

ledges were observed only occasionally and only in the later stages of precipitate growth. Thus the nucleation and the dominant mode of growth are best described by the semicoherent co-precipitation mechanism. In this description, the α platelets are C-V precipitates with one vacancy per carbon atom. The α to α' transition which occurs during aging at 400°C marks the beginning of a sequence of processes that result in the formation of the first unit cell plate of the carbide structure and its subsequent growth. Figure 6 clearly shows that the larger than average size α precipitates that are in the process of transforming to α' do so at the expense of neighboring α precipitates. The marked denuded zone (~200 nm wide) and smaller size of the α plates adjacent to transforming plates attests to this. From a consideration of the Pt_2C structure derived in paper II, it is clear that α' formation occurs when a second monolayer of vacancies condenses on the next nearest {002} matrix plane from the carbon plate. The new structure (see Fig. 8, paper II) forms if the carbon is uniformly redistributed in the tetragonal cell by the movement of half of the atoms by c/2. As noted earlier, the Pt atom relaxations accompanying this change are such that the total displacement of the lattice in the c direction is very close to a/2 <001>.

The fact that the α' grows at the expense of shrinking α plates at 400°C has interesting implications. The simplest explanation for this is that vacancies become freed as nearby α precipitates shrink, migrate to the large plate and initiate the transition. The observed distance of migration of ~200nm is in good agreement with that expected on the basis of vacancy mobility. Using the approximate relation $x = 2\sqrt{Dt}$, where x is the diffusion distance, t is the time of annealing, and $D = D^M_{IV} = a^2 \nu_{IV} \exp(S/k) \exp(-E^M_{IV}/kT)$, a value for x of 400 nm is predicted using $\nu_{IV} = 2 \times 10^{12}$ sec^{-1} (Seeger and Mehrer (11)) S = k, and $E^M_{IV} = 1.37$eV (Schüle and Scholz (12)).

Further analysis is possible by applying the dislocation loop analogy to the HVEM in-situ data on α-plate shrinkage. Assuming diffusion-controlled kinetics the shrinkage rate is given by

$$\dot{r} \simeq \frac{D_{IV}}{b} (c_1 - c_0) \qquad (1)$$

where

$$c_1 = c_0 \exp(F_c B^2/kT) \qquad (2)$$

and F_c, the driving force for shrinkage, can be equated to an effective {001} stacking fault energy γ, $B^2 = a^2/2$ is the area of a vacancy in the {001} plane, and c_0 is the equilibrium vacancy concentration at the temperature T.

Combining equations (1) and (2) gives

$$\dot{r} = \frac{D^*}{b} \exp(\gamma B^2/kT) \qquad (3)$$

since $1 \ll \exp(\gamma B^2/kT)$. D^* is the self-diffusion coefficient. Substituting the values $\dot{r}_{450} = 0.02\text{nm s}^{-1}$, b = 0.2nm, $B^2 = 7.7 \times 10^{-16}\text{cm}^2$ and $D^* = 10^{-20}\text{cm}^2\text{s}^{-1}$ (13) in Eq. 3 yields $\gamma \simeq 1100\ \text{mJm}^{-2}$. This is very high compared to usual fcc stacking fault energies of ~ 150 mJm^{-2}, but only about half the value of a typical surface or interface energy and appears to be a realistic value for the open structure of the {001} fault. It should be noted that this is the pure stacking fault energy without any involvement of carbon atoms since it was assumed that free vacancies are emitted as the α precipitates shrink. In reality, the energy of an α precipitate will be lower than that of a pure {001} stacking fault due to the stabilizing effect of the carbon. At the same time, the energy of a free vacancy is reduced by its binding to a carbon atom in a complex. Thus the activation barrier which must be overcome to produce a free vacancy from an {001} stacking fault is approximately the same as that necessary to produce a C-V complex from an α precipitate. If the diffusing species is the C-V complex, the absorption of only the vacancy required for the transition will

also deposit excess carbon in the matrix surrounding the growing α' plates.

The value for γ obtained from the 450°C shrinkage data can be used in Eq. 3 together with $D^* = 4 \times 10^{-22}$ $cm^2 s^{-1}$ (13) to estimate a shrinkage rate at 400°C of 1.5 x 10^{-3} nm s^{-1}. Complete shrinkage of precipitates of diameter d less than 11nm is predicted over the course of a 1 hr anneal making the simplest assumptions about the diffusion boundary conditions. The rate is less than that observed since $\bar{d} \simeq 35$ nm (Fig. 6) but considering the uncertainties involved the agreement is reasonable. Once all the α precipitates have dissolved, further growth or thickening of the α' will be impossible until a further supply of vacancies becomes available. This is in accordance with the observation that further changes in the precipitate structure occur only after annealing at temperatures in excess of 500°C. At this point the small voids associated with each of the α' plates become copious sources of vacancies*. Because of their proximity to the precipitates only limited diffusion is required for an emitted vacancy to collect a carbon atom and become incorporated in a precipitate growth ledge. This mechanism allows the precipitate to thicken to the α" stage and beyond depending on the local carbon and vacancy concentrations available.

In contrast to the α precipitates where shrinkage occurred rapidly at ~450°C, the α' required temperatures 60-80K higher to shrink at comparable rates. This difference reflects the increased stability of the Pt_2C structure. In terms of the loop analogy, the energy of the double {001} stacking fault is substantially reduced by the carbon atoms in their reordered configuration.

The final step in the precipitation sequence occurs when the temperature for dissolution of the carbide is reached. At this point the matrix precipitates dissolve and the autocatalytic structures associated (probably) with dislocations are the last to form before the carbon returns to solid solution.

---

*The measured mean void diameter was 15 nm. Redistribution of the vacancies contained in voids of this size into a monolayer disc would result in a vacancy loop of 100 nm diameter.

Finally, it is interesting to note that in the viewpoint of the precipitates as a Pt-C-V compound, the vacancies are an integral part of the precipitate structure. Through their collapse on {001} planes, they provide the structural change from AB to the necessary AA stacking of the precipitate structure. At the same time their excess volume helps accommodate the large increase in atomic volume (50%) accompanying the transformation. This volume effect is important and has been incorporated into theories of phase transformations (14,15). The structural effect emphasized above can be equally important and has so far been neglected. In the present case, both effects help accommodate the precipitate structure. However, this need not be the case since the two roles of vacancies are independent. For example in Al-Cu alloys during the formation of θ', isomorphous with Pt_2C, vacancies could play a similar structural role but would tend to oppose the precipitate formation through their volume effect (16).

ACKNOWLEDGEMENTS

This work was supported by the Director, Office of Energy Research, Office of Basic Energy Sciences, Materials Science Division of the U. S. Department of Energy under Contract No. DE-AC03-76SF00098. One of us (MJW) thanks the Council of the University of the Witwatersrand for the award of an overseas fellowship, and the CSIR, Pretoria, for financial support. We thank David Ackland for performing the in-situ experiments reported in Fig. 8.

REFERENCES

1. K. H. Westmacott and M. I. Perez, J. Nucl. Mat. 83, 231 (1979).
2. U. Dahmen, K. H. Westmacott and G. Thomas, Acta Metall. 29, 627 (1981).
3. S. K. Maksimov, T. I. Lukyanchuk, and M. M. Myshlayev, phys. stat. sol. (a) 24, 409 (1974).
4. L. M. Brown, R. H. Cook, R. K. Ham and G. R. Purdy, Scripta Metall. 7, 815 (1973).
5. P. Regnier, N. Q. Lam and K. H. Westmacott, Scripta Metall. 16, 643 (1982).
6. K. H.Westmacott, Cryst. Latt. Def. 6, 203 (1976).
7. A. H. Cottrell, Report on Strength of Solids (London: Phys. Soc.), 30, (1948).
8. H. Suzuki, Dislocations and Mechanical Properties of Crystals (New York: Wiley), 361 (1957).
9. R. C. Evans, Crystal Chemistry, Cambridge University Press (1966).
10. D. H. Jack and K. H. Jack, Mat. Sci. and Eng. 11, 1 (1973).
11. A. Seeger and H. Mehrer, Vacancies and Interstitials in Metals (Amsterdam: North Holland), 1 (1970).
12. W. Schüle and R. Scholz, phys. stat. sol. (b) 93, K119 (1979).
13. G. Rein, H. Mehrer and K. Maier, phys. stat. sol. (a) 45, 253 (1978).
14. K. C. Russell, Scripta Metall. 3, 313 (1969).
15. A. G. Khachaturyan, Sov. Phys.-Solid State 13, 2024 (1972).
16. U. Dahmen and K. H. Westmacott, Acta Met., submitted for publication.

Figure Captions

Fig. 1. Series of micrographs illustrating the contrast behavior of the α precipitates. With g = <111> (a) the displacement contrast is observed ($\beta = \pm 2\pi/3$) but the bounding dislocation is invisible (g.b = $\pm$ 1/3); with g = <220> (b) only two precipitate variants are imaged; both exhibit displacement contrast ($\beta = \pm 2\pi/3$) and the dislocation is in or out of contrast depending on whether g.b = + 2/3 or - 2/3; with g = <113> (c) two of the variants show the same contrast as in (a), the third shows no displacement contrast ($\beta = 2\pi$) but strong g.b = $\pm$ 1 dislocation contrast.

Fig. 2. Pair of micrographs illustrating g.b = $\pm$ 1/2 contrast behavior exhibited by α' precipitates where b = R = a/2 [001]. Strong "inside" contrast is observed in (a) and weak "outside" contrast in (b).

Fig. 3. Contrast analysis of α' precipitates. In (a) g = <111>, $\beta = \pm \pi$ and g.b = $\pm$ 1/2; in (b) g = <220>, and the two variants in contrast show no displacement contrast ($\beta = 2\pi$) but dislocation contrast, (g.b = $\pm$ 1); in (c) g = <113> and the behavior for the two variants is the same as in (a).

Fig. 4. Contrast analysis for α'' precipitates (marked A) having b = R = a[010]. Under all conditions except g.b = 0, the precipitates exhibit no (or faint residual) displacement contrast depending on s, and strong dislocation contrast.

Fig. 5. Low magnification micrographs of thick foil sections illustrating the heterogeneous structures that develop during advanced aging. In (a) the decorated dislocation structures and associated precipitate-free-zones are imaged (at 1.5MeV) while (b) shows the complex groupings that survive after the matrix precipitates have dissolved.

Fig. 6. Contrast analysis of precipitates undergoing the $\alpha \longrightarrow \alpha'$ transition. A comparison of the contrast behavior of the large precipitates with Figs. 1 and 3 shows that the outer annulus exhibits contrast consistent with α and the inner disc with α'. Note also the voids in the center of each large growing precipitate.

Fig. 7. An example of an α' to α'' transition under two diffracting conditions. A comparison with Figs. 3 and 4 shows the behavior is consistent with the outer region of the precipitate being α' and the inner α'' as illustrated in the schematic.

Fig. 8. Micrographs (a) - (d) show the regular shrinkage of α precipitates observed during in-situ isothermal annealing at 452°C. 8(e) is a microdiffraction pattern obtained from an edge-on {001} precipitate. 8(f) is a plot of the shrinkage data for several precipitates showing the shrinkage rate is constant in all cases.

Fig. 9. Sequence of micrograph (a) - (d) and graph (f) illustrating the linear shrinkage behavior of α' precipitates during annealing at 515°C. Fig. 8(e) is the microdiffraction pattern from an individual precipitate showing additional streaked spots characteristic of the Pt_2C structure.

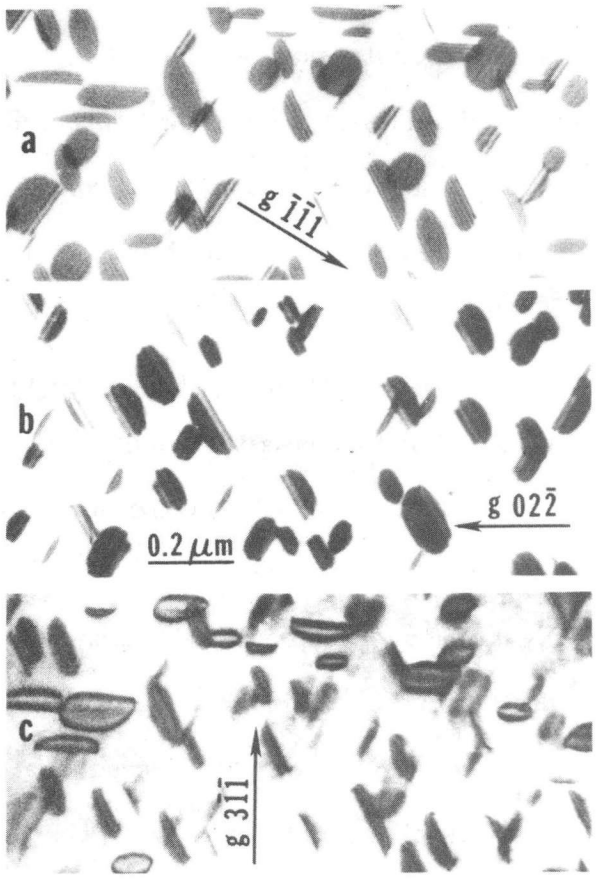

Fig. 1

XBB 827-5936

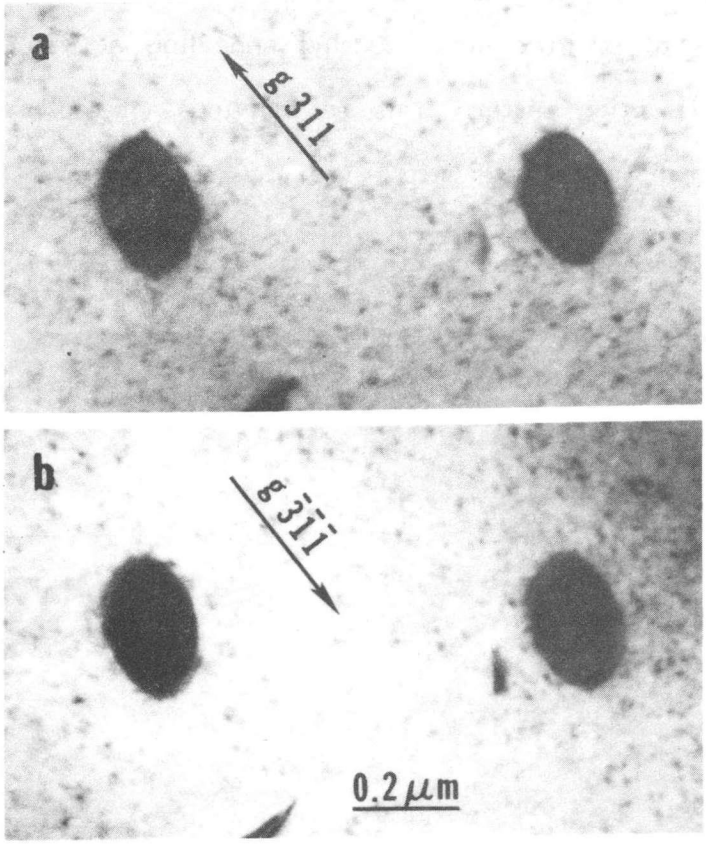

Fig. 2

XBB 827-5937

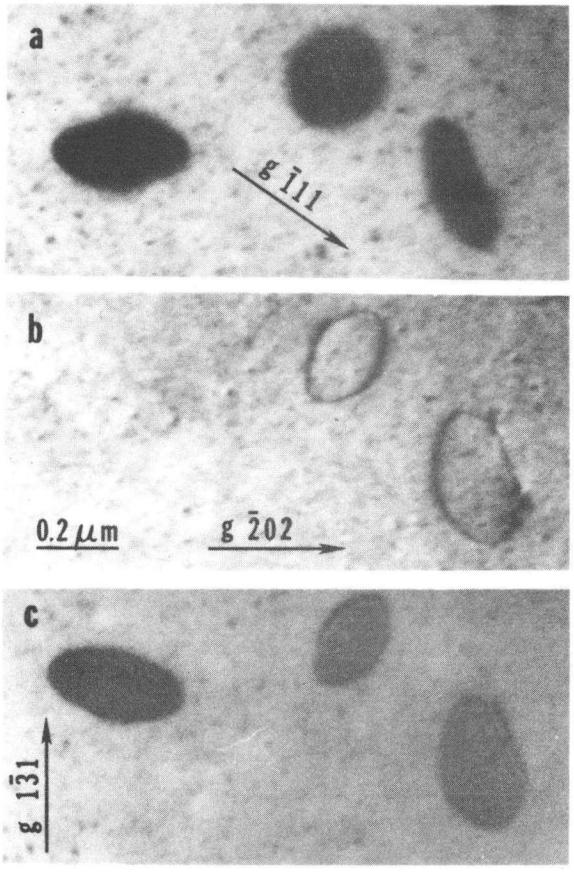

Fig. 3

XBB 827-5934

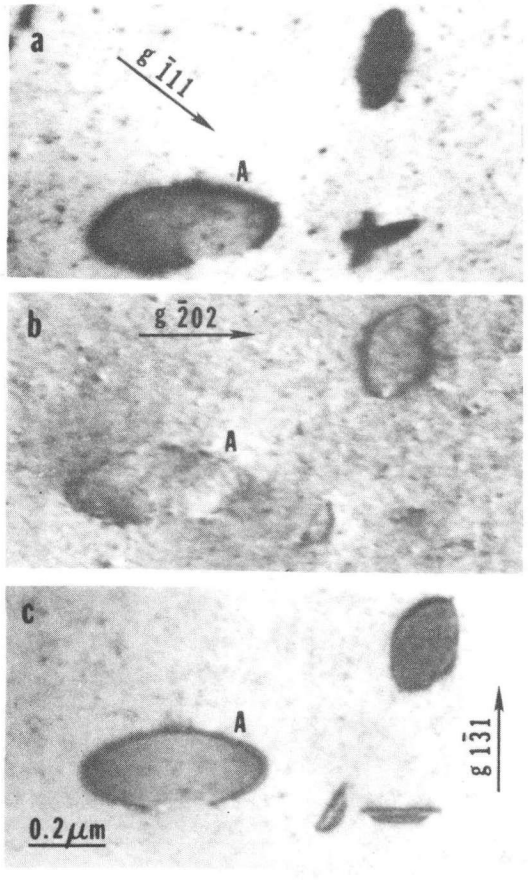

Fig. 4

XBB 827-5933

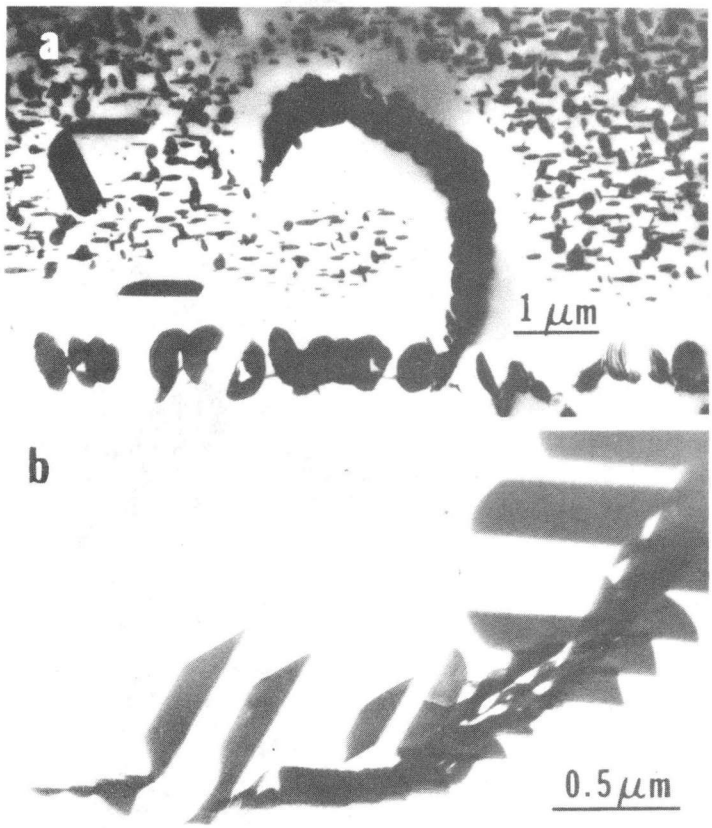

Fig. 5

XBB 827-5938

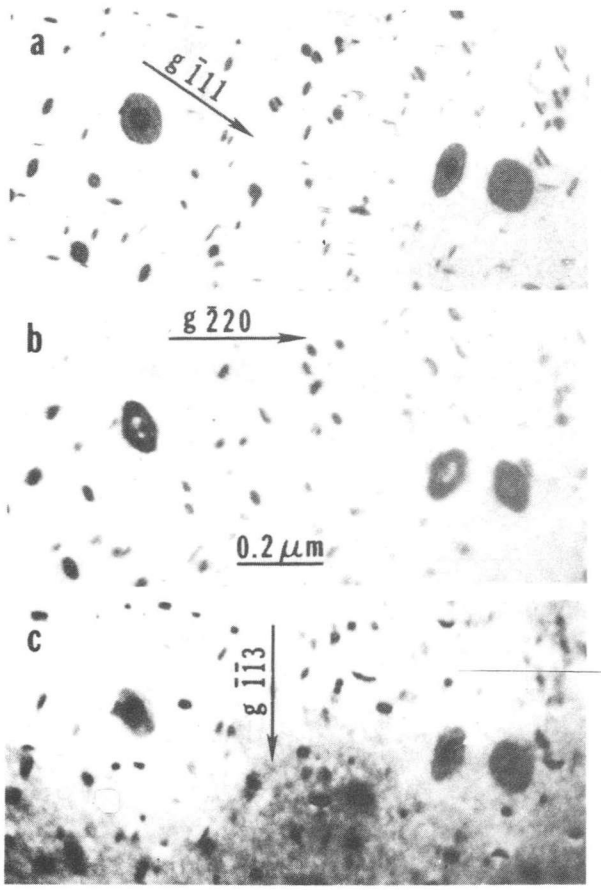

Fig. 6

XBB 827-5932

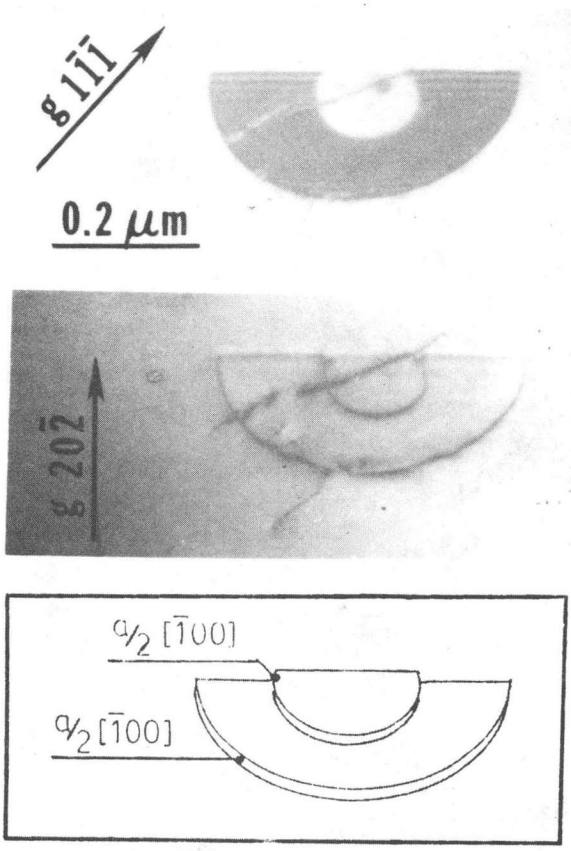

Fig. 7

XBB 827-5931

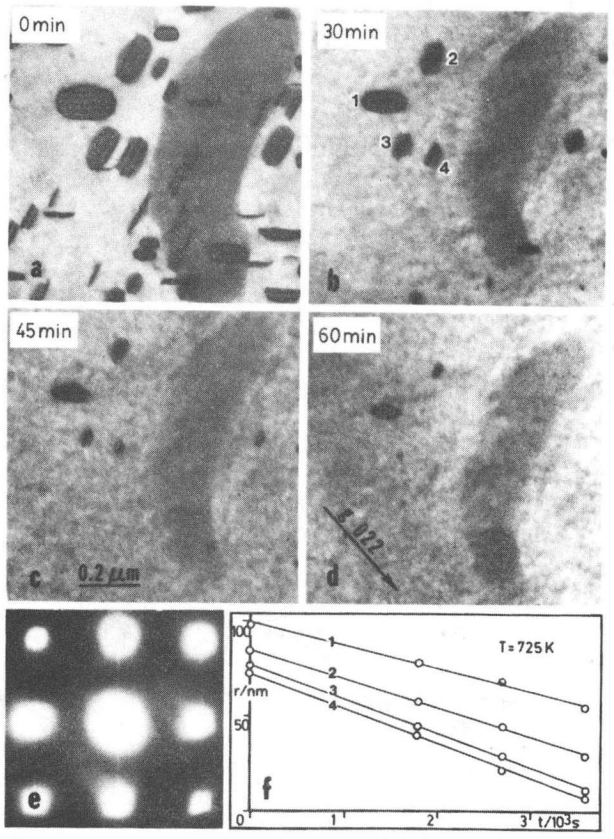

Fig. 8

XBB 827-5929

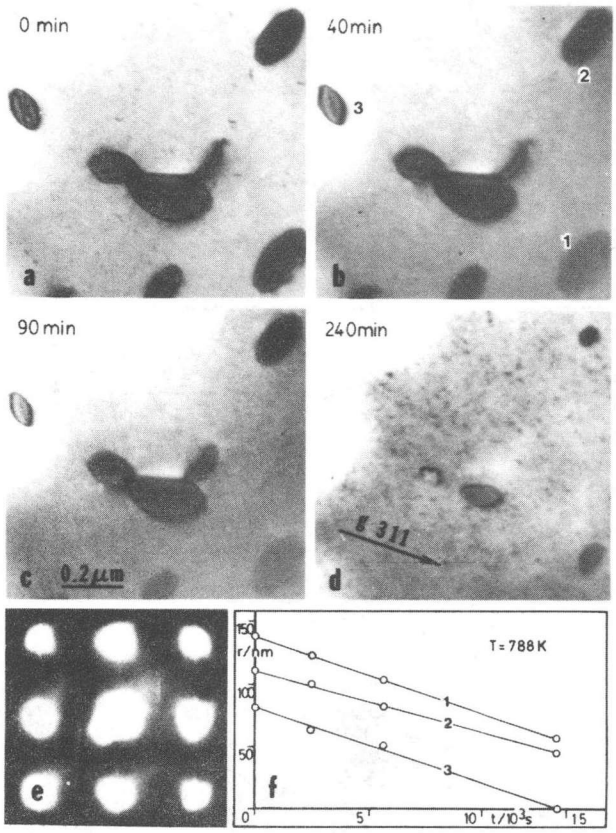

XBB 827-5928

Fig. 9

TECHNICAL INFORMATION DEPARTMENT
LAWRENCE BERKELEY LABORATORY
UNIVERSITY OF CALIFORNIA
BERKELEY, CALIFORNIA 94720